SUPPORTING INFORMATION

Linker-Induced Anomalous Emission of Organic-Molecule Conjugated Metal-Oxide Nanoparticles

Volodymyr Turkowski[ψ,χ], Suresh Babu[α], Duy Le[ψ], Amit Kumar[§], Manas K. Haldar[Φ], Anil V. Wagh[Φ], Zhongjian Hu[ψ], Ajay S. Karakoti[¥], Andre J. Gesquiere[ψ,μ,β], Benedict Law[Φ], Sanku Mallik[Φ], Talat S. Rahman[ψ,χ], Michael N. Leuenberger[ψ,χ], Sudipta Seal[,χ,§]*

[ψ]Department of Physics, [χ]NanoScience Technology Center, [§]Advanced Materials Processing and Analysis Center, [μ]Department of Chemistry, [β]College of Optics and Photonics, University of Central Florida, Orlando, FL -32816, USA

[α]Centre for NanoScience and Technology, Madanjeet School of Green Energy Technologies, Pondicherry University, Pondicherry – 605 014, India

[Φ]Department of Pharmaceutical Sciences, North Dakota State University, Fargo, ND, USA

[¥]Environmental and Molecular Sciences Laboratory, PNNL, Richland, WA-99354, USA

SI 1: The FTIR spectra are depicted for TiO_2, TiO_2-APTMS and TiO_2-APTMS/FA conjugated nanoparticles. In pure TiO_2, the characteristic bands at 3400 and 1634 cm^{-1} correspond to that of hydroxyl groups (OH bending vibration) indicating surface adsorbed hydroxyl groups (Reference 1-SI). Upon APTMS functionalization of TiO_2 distinctive bands appeared at 2926 and 2877 cm^{-1} corresponding to symmetric and as asymmetric stretch of C-H respectively (Reference 2-SI). The band observed at 1607 cm^{-1} is the bending mode of NH- vibration and the peak at 1513 cm^{-1} corresponds to the characteristic phenyl ring present in the folic acid (Reference 3-SI). The band at 1195 cm^{-1} observed for TiO_2-APTMS/FA is attributed to C-N stretching. The peak due to C=O (1700 cm^{-1}) stretching appears upon folic acid conjugation of TiO_2-APTMS, indicating the formation of TiO_2-APTMS/FA conjugation in the sample.

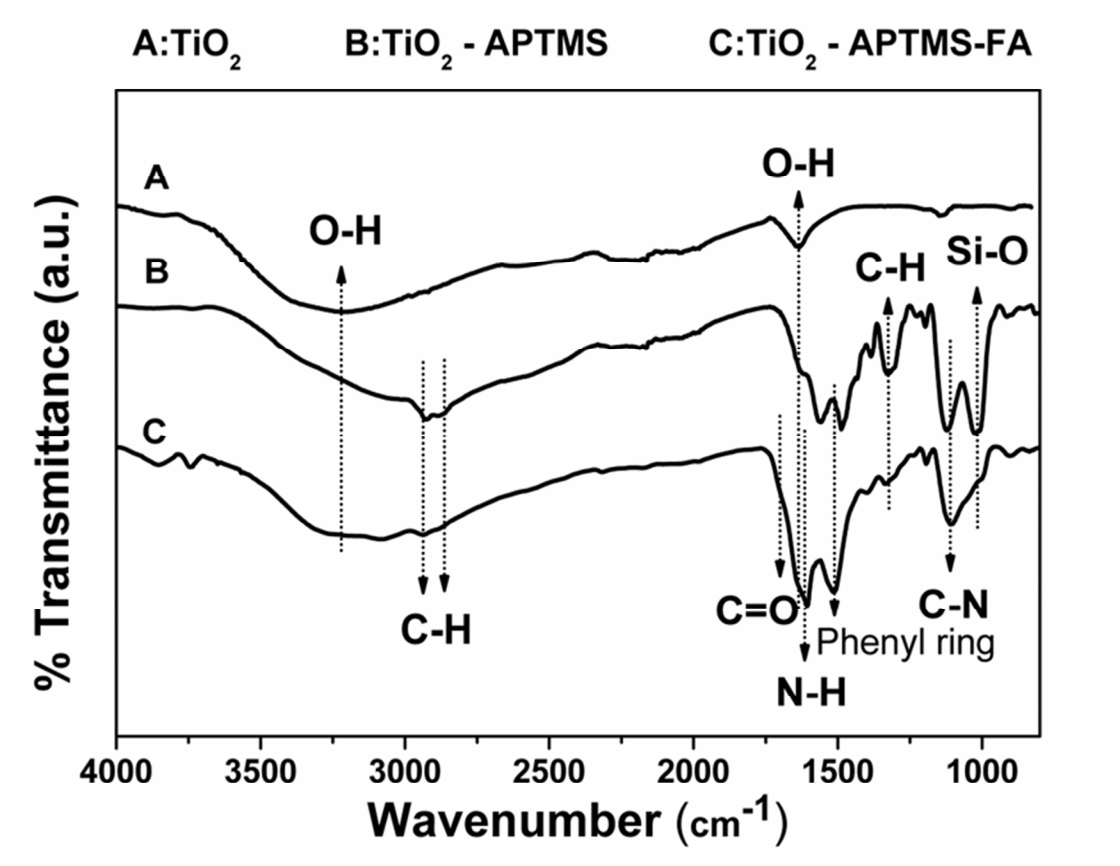

SI 2.1 –X-ray Photoelectron Spectroscopy (XPS) is a common surface analysis technique (References 4-SI-10-SI) adopted by many researchers for analyzing the surface chemistry of organic-inorganic interaction and functionalization. In this study, the XPS measurements were performed using PHI 5400 system with a monochromatized Al Kα source. Before recording XPS, the binding energy was calibrated with respect to Au 4f7/2 core level at 83.9 eV±0.05 eV. Samples were exposed to minimum radiation in order to avoid any potential beam damage to the materials. The multiplex high resolution scans obtained from XPS were charge corrected to carbon (C1s) at 284.6 eV (Reference 11-SI) for further analysis in calculating binding energy shifts identify the nature of the functional groups and bonding. (a) The survey spectra for TiO2 and TiO2-APTMS-FA reveals the appearance of Si and N peak (shown as inset (N(1s) for clarity) upon functionalization of TiO_2 to TiO_2-APTMS-FA. (b) XPS spectra for Ti 2p in TiO_2-APTMS-FA sample show the splitting of Ti 2p peak (Reference 12-SI). (c) The N 1s spectrum of TiO_2-APTMS/FA was deconvoluted using a peak-fit 4.0 software to show the presence of different chemical environment around N (please refer to the schematic diagram) to identify the presence of functional groups resulting from functionalization. The peak fitting was done in a similar manner as published before (Reference 13-SI), briefly, Shirley background correction was performed on the XPS spectrum, followed by fitting to Gaussian-Lorentzian peak shapes. The N 1s reveals peak (Reference 14-SI) at (402.1 eV) corresponding to N in the ring and the peak at 399.1 eV corresponds to N-C=O, both of which are present in TiO_2-APTMS-FA as depicted in the schematic diagram. The other peaks of N appear at 400.5 eV and 399.9 eV corresponding to N-C and N-H bonds. (d) The Si 2p spectrum of TiO_2-APTMS-FA shows the presence of Si-C bonds (100.6 eV eV) and Si-O-Ti (102.5 eV). The Si peak at 103.8 eV corresponding The Si-O peak in TiO_2-APTMS shifts to 102.5 eV (Si 2p peak in SiO_2 is 103.5 eV) corresponding to Si-O-M as explained in an earlier publication, where M is a non-negative element (when M is a metal cation, M-O bond is relative ionic which forces the Si-O bind to become more covalent than SiO_2) (references 15-SI, 16-SI). The shift observed in the Si-O bond of TiO_2-APTMS-FA, further suggests the functionalization chemistry.

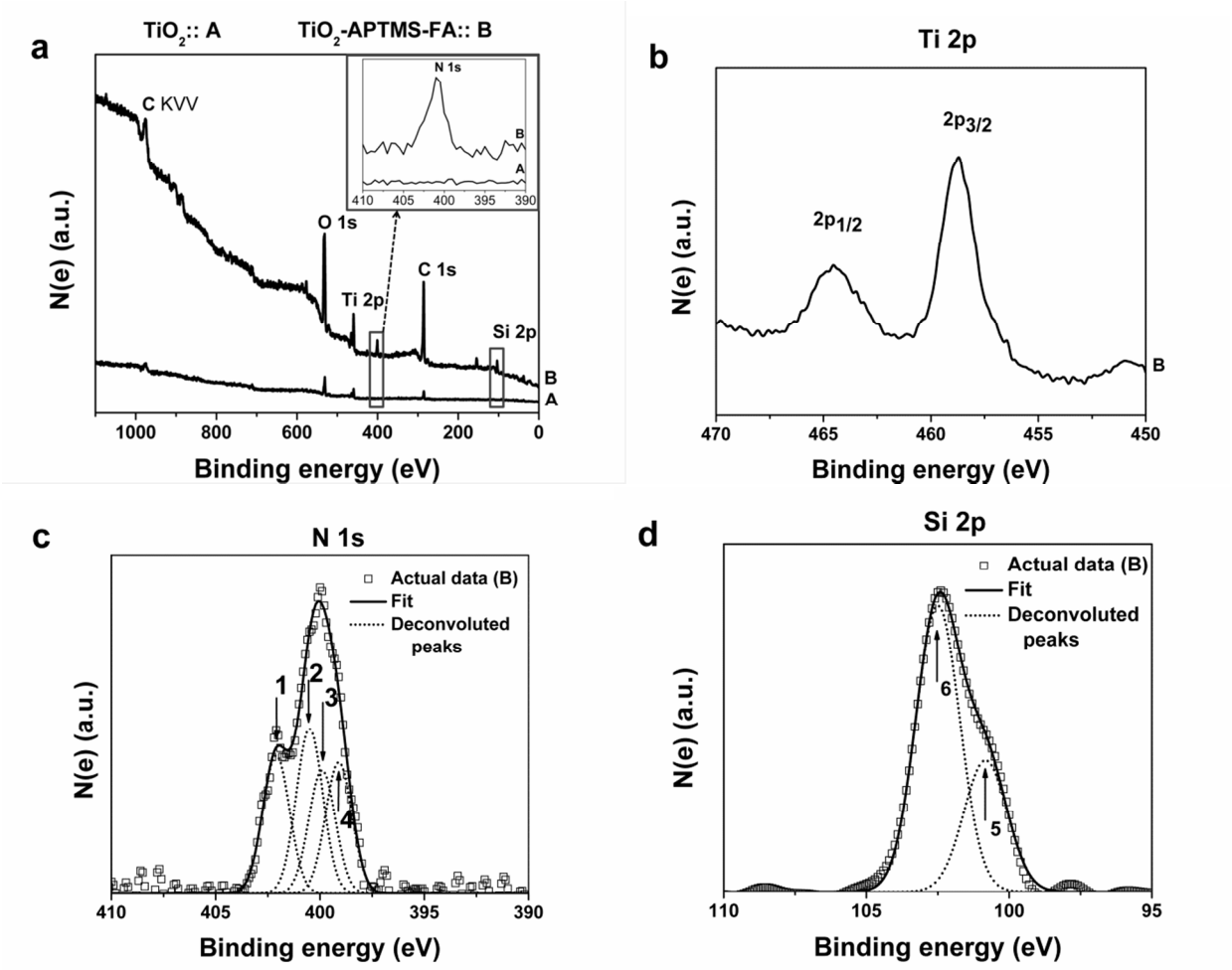
a
TiO2:: A
TiO2-APTMS-FA:: B
C KVV
O 1s
Ti 2p
C 1s
Si 2p
N 1s
B
A
N(e) (a.u.)
Binding energy (eV)
b
Ti 2p
2p3/2
2p1/2
c
N 1s
Actual data (B)
Fit
Deconvoluted peaks
d
Si 2p


e
TiO2
Folic acid

SI-2.2: Elemental analysis of TiO_2-APTMS-FA was carried out using energy-dispersive X-ray spectroscopy

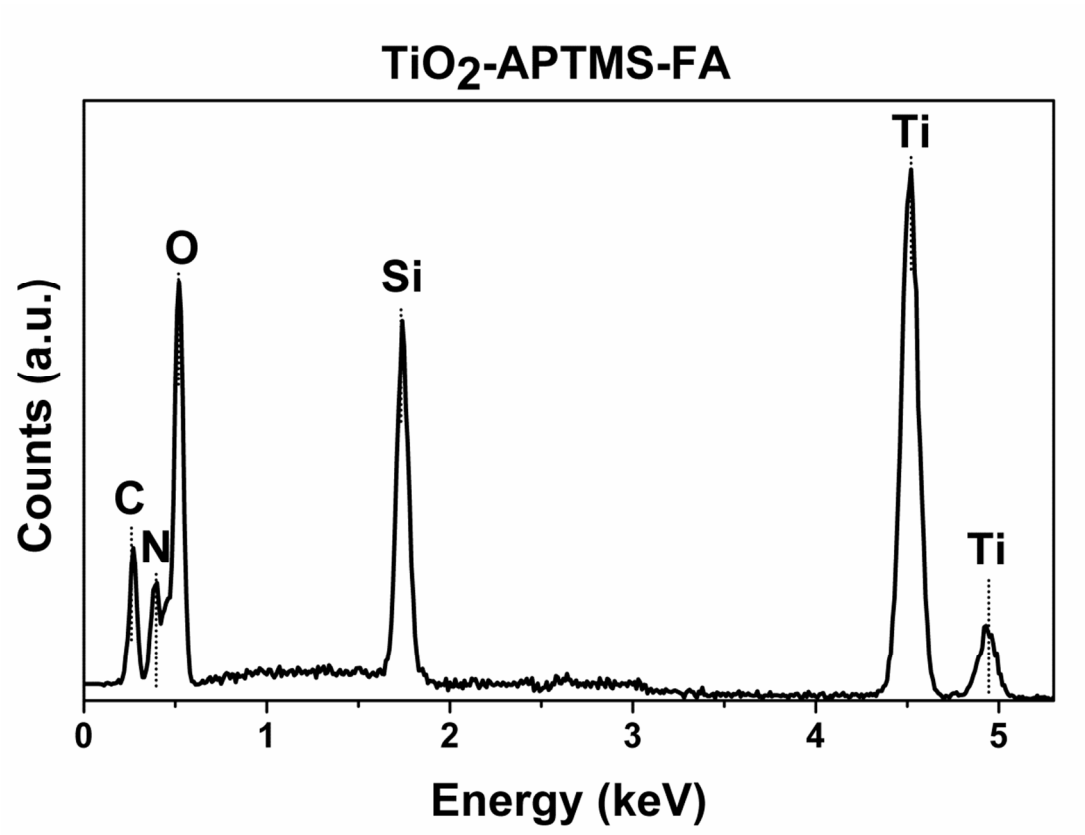

SI-3 - High resolution TEM images of as prepared titania nanoparticles (a, b) depicting the size in the range of 7-10 nm. Upon conjugating TiO_2 nanoparticles with APTMS and FA, the nanoparticles appear less agglomerated and the size of nanoparticles remained unchanged (c, d).

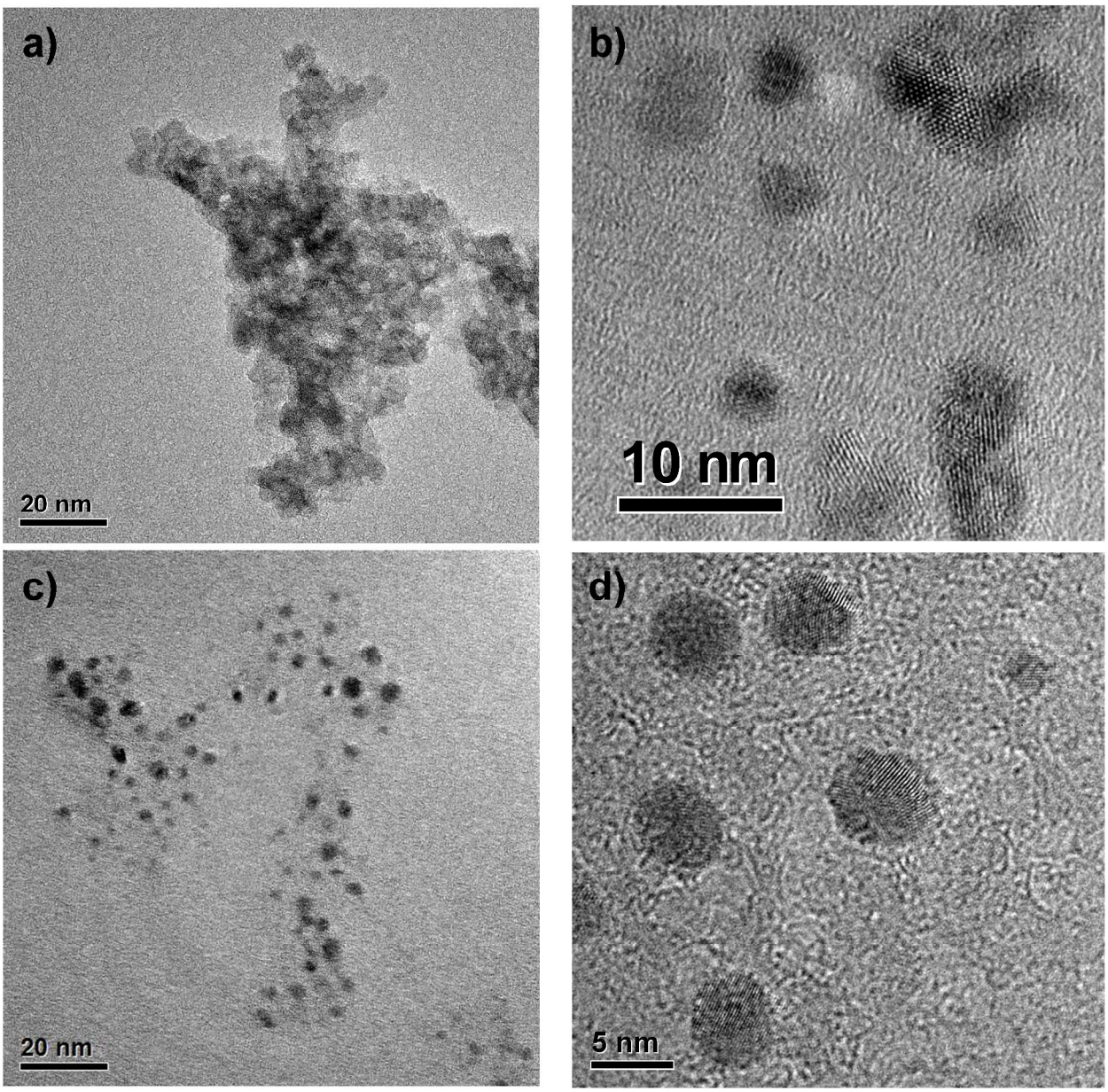

SI-4 Computational details

For the numerical analysis we used both TDDFT and DFT approaches. Namely, the optimized structure of the FA and APTMS/FA molecules were obtained from the DFT analysis by using the Gaussian03 code[23] with the B3LYP exchange-correlation[24-26] potential and the 6-31G(d) basis set in the case of FA and APTMS molecules. We have shown by using several GGA potentials that the results are stable with respect to the choice of the XC potential The TDDFT extension of this approach was used to calculate the excited energy levels and the transition moments for these molecules. The analysis of the TiO_2, TiO_2-APTMS and APTMS-TiO_2/FA systems was performed by using the DFT calculations with the VASP 4.6 code with GGA-PAW potentials, including the GGA+U case[17-SI]. In order to study the surface properties of the TiO_2 nanoparticle, it was modeled by a 239-atom five-layer slab with two (110) surfaces. We have used the energy cut-off of 400eV and the Brillouin zone has been sampled according to the Monckhorst-Pack scheme[18-SI] with the shrinking factors of three in the surface plane directions and one in the out-of-plane direction.

SI 5 – Optimized structures for the APTMS and FA molecules. The red, yellow, grey and small blue balls are oxygen, carbon, nitrogen and hydrogen atoms, correspondingly. The large blue ball in the APTMS is a silicon atom.

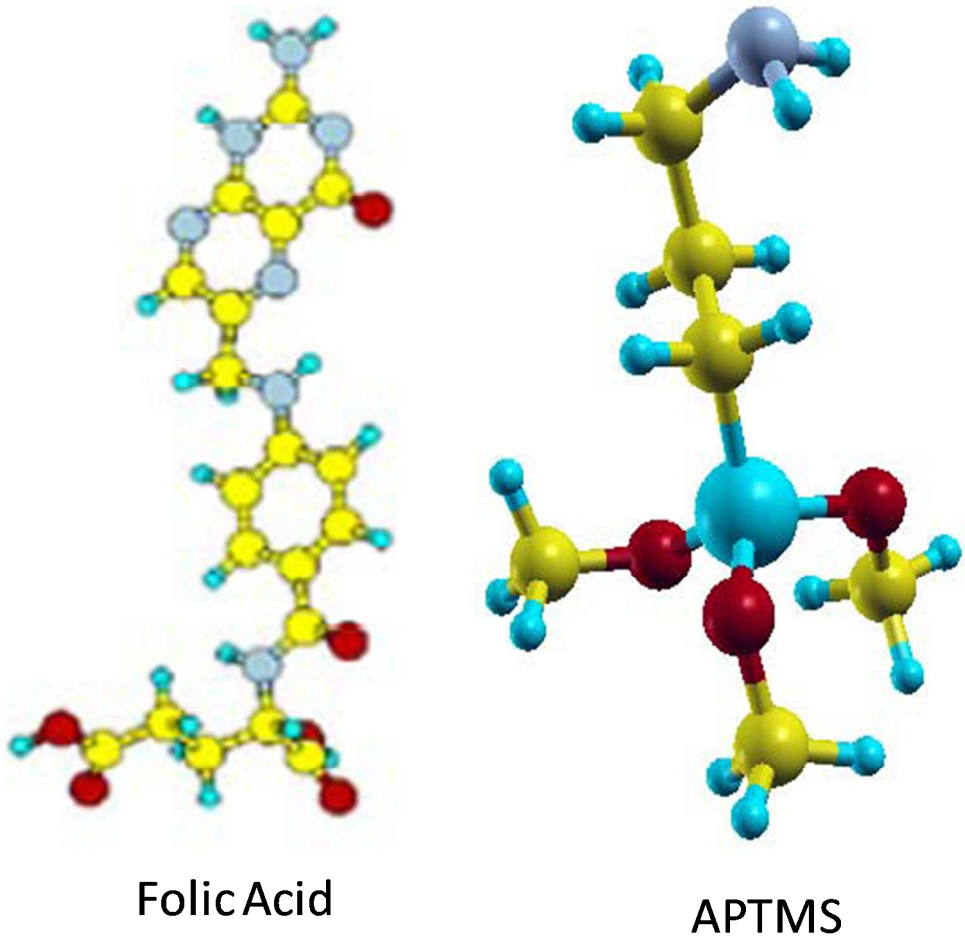

SI-6.1. Details of the analysis of the PL mechanism

Calculations demonstrate that the OVs may tend to occupy a subsurface layer (with an energy lower than that of the surface bridge sites[28]). However, these states are also pretty close to the oxygen bridges where APTMS anchors have to be attached to the oxygen bridge row of the (110) surface through two-oxygen coupling. After the coupling, one of the three OCH_3 groups remains on the molecule, while the other two are detached and bind to the surface Ti sites. Since the OVs and the APTMS oxygen atoms, which bind to the surface, are on the same oxygen-bridge rows, the vicinity enables excitation of these electrons to the molecular states and also facilitates trapping of the OV electrons by the APTMS/FA holes. Such processes do not take place in cases in which the molecule is attached to atoms far from the bridges (in TiO_2-FA, for example, FA is attached to a titanium atom). In Fig.5 we present the densities of states and the scheme of the PL mechanism due to transition between the molecule-OV and molecule-molecule levels (details are given in caption to the Figure 1). In particular, since the lifetime of the holes on the APTMS/FA levels (M1-M5) below the molecular HOMO state (M6) considered in case (1) is much shorter than the lifetime of the holes in the molecular HOMO state (M6), mechanism (2) has to be considered as the dominant one. It is important to note that the latter value for the molecular excited lifetime of NP-APTMS/FA is significantly larger than the experimental result for the folic acid molecule (~10 ns, see Refs.32-33). This can be explained by an increase of the spatial separation between the charge distribution for the molecular HOMO and LUMO states due to the APTMS molecule. The schematic PL mechanisms are presented in Figures 3e,f. Theoretically calculated PL of the TiO2, TiO2-APTMS and TiO2-APTMS/FA is presented in Fig. 3g. Clearly, our calculations agree with the experimental data (Fig. 2c and SI-6) reasonably well. In particular, given a large molecular coverage, the TiO2-APTMS spectrum is shifted to higher energies with respect to that of bare TiO_2. Our calculations show that the OV state extends rather far inside the APTMS molecule (Fig. SI-6.2) which makes the OV to APTMS/FA excitations and the electron-hole recombination favorable. Since the FA molecule couples to Ti sites through two oxygen atoms (bottom part of the FA, Fig. SI-5) without any linker molecule, the FA holes are far from both the surface oxygen bridges and the OV electron states of titania, resulting in decreasing the probability of electron-hole recombination and consequently a reduced PL.

Figure SI-6.2 – Charge distribution of the spin-up TiO_2-APTMS/FA states relevant to the PL mechanism. The results were obtained by using the VASP 4.6 code with GGA-PAW potentials.[26] The different pictures correspond to the following states: a) the OV state N1; b) the LUMO-1 (M5) state of APTMS/FA; c) the superposition of the OV states N2 and N3; d)-e) HOMO (M6) and LUMO (M7 and M8) states of the APTMS/FA; f) the APTMS-FA LUMO+1 (M9) and g) TiO_2 excited states (N4). As it follows from these Figures, due to vicinity of the OV states to the molecule, the probability of the charge transfer from the OVs to the molecule increases. The main contribution to the PL comes from the de-excitation process from the LUMO (e) to HOMO (d) in the APTMS/FA subsystem.

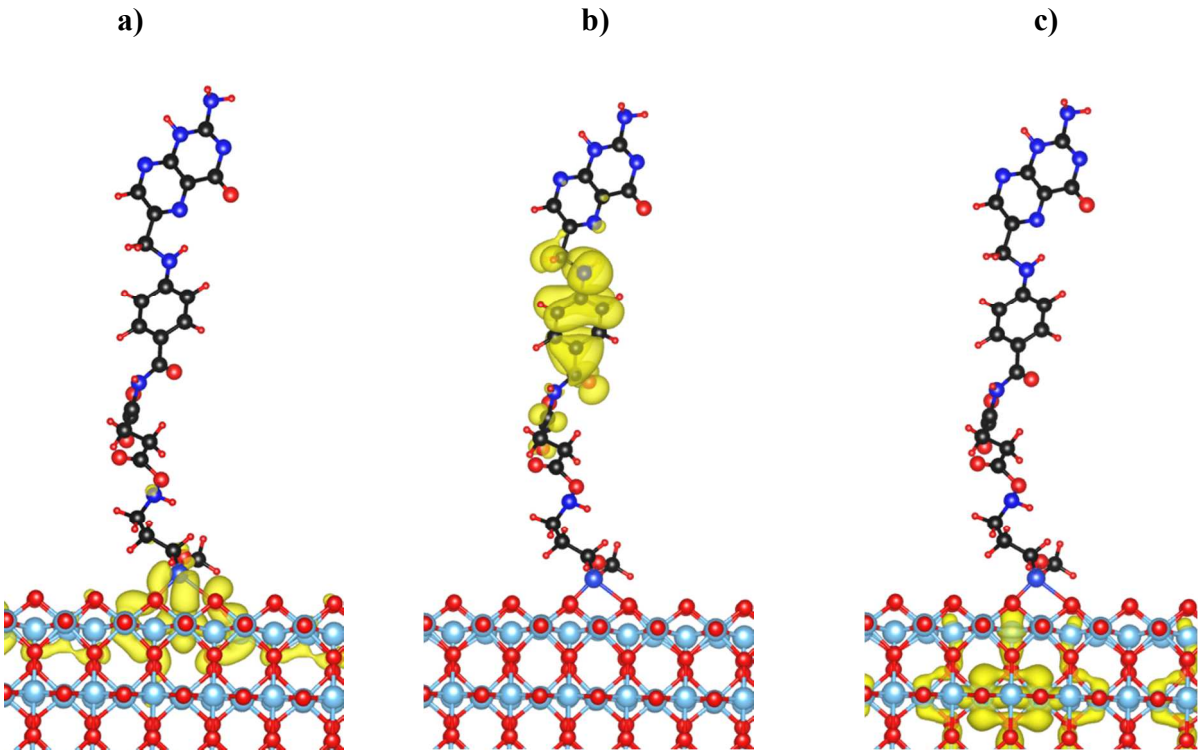

d)

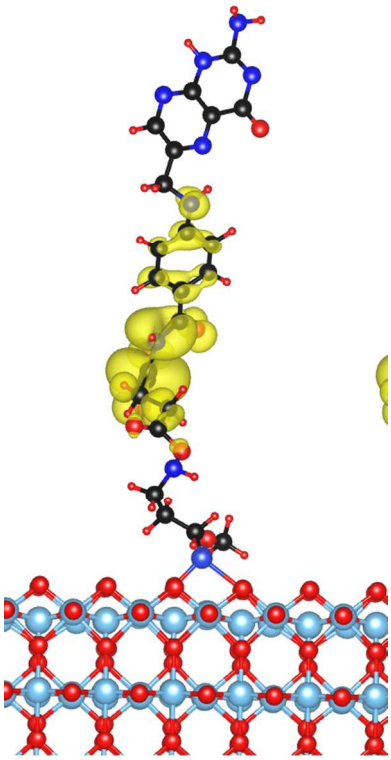

e)

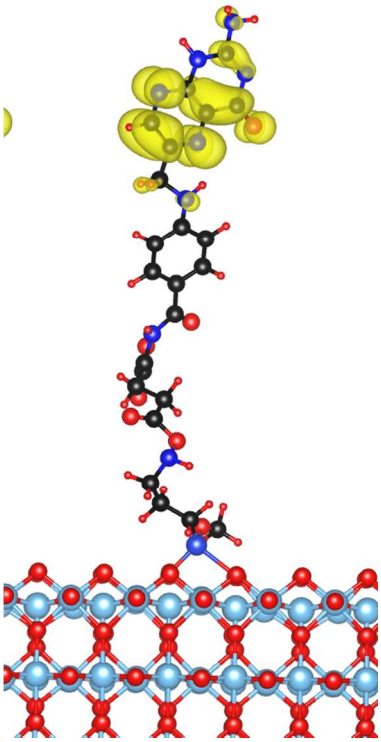

f)

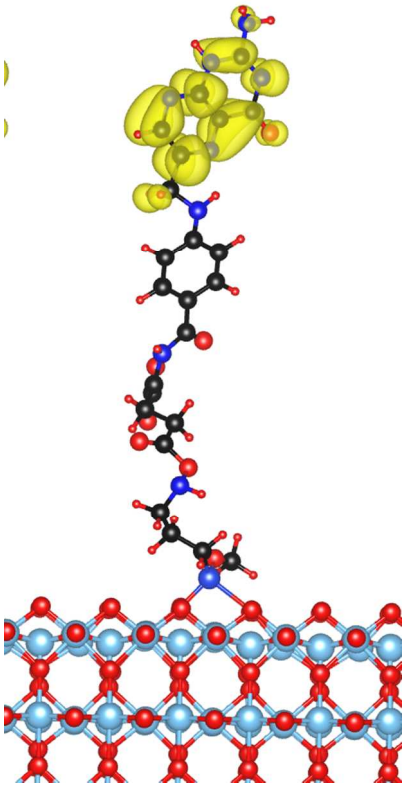

g)

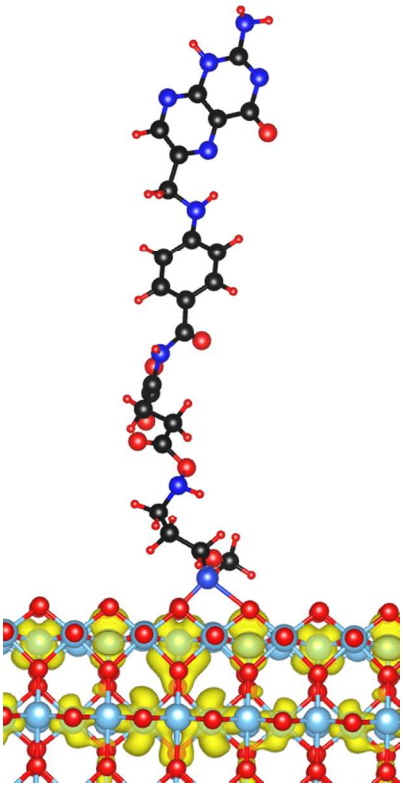

SI-7 Estimation of the quantum yield

In the case of photoemission, the quantum yield is defined as the ratio of number of emitted photons (see, for example Ref. 19-SI) to the number of absorbed photons. In our case, the 465nm photons can be mainly absorbed through two channels:

1) OV to the molecular orbital transition
2) Molecular HOMO to higher excited state transitions.

The calculations of the transition oscillator strengths give the following ratio for two cases: f_1:f_2=7.23:1.0. Since the first process, is the main channel which leads to the photoemission, we may estimate that 7.23/(7.23+1.0)~87.8% of the absorbed photons will contribute to the photoemission. Next, the LUMO excited electrons can recombine either with a) the OV hole or b) with the molecular HOMO hole (the recombination times ratio t_b/t_a=49.6 can be estimated from the formula $t_i \approx \frac{c^3}{2\Delta E_i^{\,2} f_i}$ presented also in the main text). Channel b is mostly responsible for the visible PL. Therefore, the quantum yield can be estimated as $0.878\frac{1}{1+t_b/t_a} = 86\%$. It must be noted that this an estimation, and more accurate calculations including the inter-molecular interaction and the contribution from anatase nanoparticles may result in ~10% correction of this result.

REFERENCES

(1-SI) Bernath, P.F. The Spectroscopy of Water Vapour: Experiment, Theory and Applications. *Phys. Chem. Chem. Phys.* ***2002,*** *4,* 1501-1509.

(2-SI) Park, H.D.; Park, S.S.; Choe, S.J. The Formation of Metal (M=Co(Ⅱ), Ni(Ⅱ), and Cu(Ⅱ)) Complexes by Aminosilanes Immobilized with Mesoporous Sieves. *Bull. Korean Chem. Soc.* ***1999,*** *20,* 291.

(3-SI) He, Y.Y.; Wang, X.C.; Jin, P.K.; Zhao, B.; Fan, X. Complexation of Anthracene with Folic Acid Studied by FTIR and UV Spectroscopies. *Spectrochim. Acta, Part A.* ***2009,*** *72,* 876-879.

(4-SI) Patil, S.; Reshetnikov, S.; Haldar, K.; Seal, S.; and Mallik, S. Surface Derivatized Nanoceria with Human Carbonic Anhydrase II Inhibitors and Fluorophores: a Potential Drug Delivery Device. *J. Phys. Chem. C.* ***2007,*** *111,* 8437-8742.

(5-SI) Singh, S.; Kumar, A.; Karakoti, A.; Seal, S.; and Self, W.T. Unveiling the Mechanism of Uptake and Sub-Cellular Distribution of Cerium Oxide Nanoparticles. *Mol. BioSyst.* ***2010,*** *6,* 1813-1820.

(6-SI) Wan, D.; Yuan, S.; Neoh, K.G.; and Kang, E.T. Surface Functionalization of Copper *via* Oxidative Graft Polymerization 2,2′-biothiophene and Immobilization of Silver Nanoparticles for Combating Biocorrosion. *Applied Materials and Interfaces* ***2010,*** *2,* 1653-1655.

(7-SI) Recio-Sánchez, G.; Domínguez-Cañizares, G.; Manso, M.; Preda, I.; Torres-Costa, V.; Gutiérrez, A.; Soriano, L.; and Martín-Palma, R.J. Surface Functionalization of Nanostructure Porous Silicon by APTs: Toward the Fabrication of Electrical Biosensors of Bacterium Escherichia Coli. *Current Nanoscience.* ***2011,*** *7,* 178-182.

(8-SI) Simpkins, B.S.; McCoy, K.M.; Whitman, L.J.; and Pehrsson, P.E. Fabrication and Characterization of DNA-Functionalized GaN Nanowires. *Nanotechnology.* ***2007,*** *18,* 355301.

(9-SI) Singh, S.; Sharma, S.N.; Govind; Shivaprasad, S.M.; Lal, M.; and Khan, A.M. Nanostructured Porous Silicon as Functionalized Material for Biosensor Application. *J. Mater. Sci.: Mater. Med.* ***2009,*** *20,* 181.

(10-SI) Salvagnini, C.; Roback, A.; Momtaz, M.; Pourcelle, V.; Marchand-Brynaert, J. Surface Functionalization of Poly(butylene terephthalate) (PBT) Melt-Blown Filtration Membrane by Wet Chemistry and Photo-Graftion. *J. Biomater. Sci., Polym. Ed.* ***2007,*** *18,* 1491.

(11-SI) Barr, T. L.; Seal, S. Nature of the Use of Adventitious Carbon as a Binding Energy Standard. *J. Vac. Sci. Technol., A.* ***1995,*** *13*, 1239-1246.

(12-SI) Kurtz, R. L.; and Henrich, V. E. Comparison of Ti 2p Core-Level Peaks from TiO_2, Ti_2O_3 and Ti Metal by XPS. *Surf. Sci. Spectra.* ***1998,*** *5,* 179-181.

(13-SI) Kumar, A.; Babu, S.; Karakoti, A.S.; Schulte, A.; Seal, S. Luminescence Properties of Europium-Doped Cerium Oxide Nanoparticles: Role of Vacancy and Oxidation States. *Langmuir.* ***2009,*** *25,* 10998-11007.

(14-SI) Wagner, C. D. Handbook of X-ray Photoelectron Spectroscopy. *Perkin-Elmer Corp., Physical Electronics Division,* ***1979.***

(15-SI) Seal, S.; Krezoski, S.; Hardcastle, S.E.; Barr, T.L.; Petering, D.H.; Cheng, C.-F.; Klinowski, J.; Evans, P.H. Investigations of the Surface Chemistry of Pathogenic Silicates. *Journ. of Vac. Sci. and Tech. A.* ***1995,*** *13,* 1260-1266.

(16-SI) Seal, S.; Krezoski, S.; Petering, D.; Barr, T. L.; Klinowski, J.; Evans, P. X-ray Photoelectron Spectroscopy Investigations of the Interaction of Cells with Pathogenic Asbestoses. *Journ. of Vac. Sci. and Tech. A.* ***1996,*** *14*, 1770-1778.

(17-SI) Kresse, G.; Hafner J. Computer Code VASP Guide. University of Vienna, **2003**.

(18-SI) Monkhorst, H.J.; Pack, J.D. Special Points for Brillouin-Zone Integrations. *Phys. Rev. B: Condens. Matter Mater. Phys.* **1976**, 13, 5188-92.

(19-SI) Skillman, J.B. Quantum Yield Variation Across the Three Pathways of Photosynthesis: not yet Out of the Dark. *J. Exp. Bot.* ***2008****, 59,* 1647-1661.